

# TM oxides coatings for high demanding accelerator components

J. Scifo<sup>1</sup>, A. Marcelli<sup>1,2</sup>, B. Spataro<sup>1</sup>, D. Hampai<sup>1</sup>, S. Dabagov<sup>1</sup>, S. Sarti<sup>3</sup>, A. Di Trollo<sup>1,4</sup>,  
R. Moscatelli<sup>5</sup> and S. Macis<sup>6,1</sup>

<sup>1</sup>INFN - Laboratori Nazionali di Frascati, P.O. Box 13, 00044, Frascati, Italy

<sup>2</sup>RICMASS, Rome International Center for Materials Science Superstripes, 00185 Rome, Italy

<sup>3</sup>Dipartimento di Fisica, Università di Roma "La Sapienza", P.le A. Moro 2, 00185 – Rome, Italy

<sup>4</sup>CNR-Istituto di Struttura della Materia, via Salaria km 29,500, 00015 Monterotondo St. (Roma)

<sup>5</sup>Department of Engineering, Università Roma Tre, Via Vito Volterra 62, 00146 – Rome, Italy

<sup>6</sup>Università di Tor Vergata, Via della Ricerca Scientifica 1, 00133 Roma, Italy

## Abstract

Large electric gradients are required for a variety of new applications, notably including the extreme high brightness electron sources for X-ray free electron lasers (FELs), RF photo-injector, industrial and medical accelerators and linear accelerators for particle physics colliders. In the framework of a INFN-LNF, SLAC (USA), KEK (Japan), UCLA (Los Angeles) collaboration, the Laboratori Nazionali di Frascati (LNF) is involved in the modelling, development and test of RF structures devoted to acceleration with high gradient electric field of particles through metal device. In order to improve the maximum sustainable gradients in normal conducting RF accelerating structures, we had to minimize the breakdown and the dark current. To this purpose the study of new materials and manufacturing techniques is mandatory to identify solutions to such extremely demanding applications. We considered the possibility to coat copper (and other metals) with a relatively thick film to improve and optimize breakdown performances. We present here the first characterization of MoO<sub>3</sub> films deposited on copper by pulsed-laser deposition (PLD) starting from a commercial MoO<sub>3</sub> target.

Key words: WORK FUNCTION, BREAKDOWN, TM OXIDES, RF STRUCTURES.

PACS: 68.00.00, 68.35.Ct, 77.84.Bw, 96.50.Pw, 81.05.-t, 81.15.-z

PHYSICS AND APPLICATIONS OF HIGH BRIGHTNESS BEAMS Crete, April 8-12, 2019

Work supported by INFN National Scientific Committee 5

## 1 – INTRODUCTION

Among the many metals used in the industry and in the technology, copper is certainly not a critical resource, not for lack of importance, but because supply risks at present are low<sup>1)</sup>. However, a better use of copper has to be considered in many applications, e.g., copper is a strategic material for the R&D of RF cavities and other accelerating components<sup>2)</sup>. Many researches have been already devoted to develop new copper-based technologies<sup>3,4)</sup> and we are also working to improve the performance of copper based devices used in accelerator technologies that experience high accelerating gradients. In the design of new linear accelerators optimized for high brilliance photon sources, e.g., the coherent x-ray sources also known as free electron lasers (FELs), the electrical gradient is certainly one of the main parameters<sup>5,6)</sup> not only because affects the cost of the project, but because it may establish the real feasibility. Indeed, the main limitation of high accelerating gradients is the breakdown phenomenon that occurs inside RF cavities damaging surfaces and with dramatic changes in the transmission and reflection of the RF power. Breakdown is a phenomenon, which limits the performance of any accelerators. The loss of the stored energy is one of the practical results. Although breakdown may be initiated locally at the metallic surface, effects propagate across the entire cavity. During a breakdown event, part of the stored energy in the cavity is directed towards the wall, and localized surface melting occur. Various mechanisms have been considered responsible<sup>7)</sup> for initiating RF breakdown but no agreement on the cause exists due to the rapid and unpredictable nature of the observed process<sup>8-10)</sup>. However, the quality of the RF surface has been recognized as a major factor contributing to RF breakdown. Surface defects and impurities contribute as emission sites that induce important local field enhancements. Nevertheless, from an engineering point of view the surface characteristics necessary to reach a defined accelerating gradient avoiding the irreversible surface damage to high power RF components and RF sources are not defined<sup>11)</sup>. The present accelerators work at gradients of 15-20 MV/m, but tests are in progress with X-band devices working at 65 MV/m<sup>12)</sup>. About the future, the CERN based Compact Linear Collider (CLIC) design requires RF cavities with a gradient of  $\sim 100$  MV/m at 12 GHz<sup>13)</sup>. As a consequence, an increasing number of studies are looking at the characterization of the metallic surfaces of the accelerator components and discussed the use of possible coatings to improve the properties of copper. Recently a manuscript by Belli et al.<sup>14)</sup> showed that minimizing the thickness of the coating layer is mandatory to increase the single bunch instability thresholds in the proposed lepton collider at 45.6 GeV. Also for this reason, coatings have been investigated at CERN by means of numerical simulations and experimental tests with the purpose of finding an optimal thickness<sup>14)</sup>. Actually, the next generation of linear accelerators is highly demanding in terms of accelerating gradients. The experience shows that obtaining high gradients with a normal conducting structure requires operation at a relatively high frequency. As a consequence to make possible the construction of the future high-energy linear accelerators and X-ray Free Electron Lasers (FEL) and minimize costs, in addition to advanced RF devices also high frequency accelerating structures are required. To develop components with performances well beyond the existing copper based device, is fundamental to use significantly improved manufacture



technologies and surface characterization methods. Technological activities to design, manufacture and test new accelerating devices using different materials and methods are under way all over the world. In the frame of the collaboration with INFN-LNF/SLAC/KEK concerning breakdown studies about RF high gradient accelerating structures working at 11.424 GHz, an extensive R&D activities concerning materials and copper coatings are in progress at the Laboratori Nazionali di Frascati<sup>(5,16)</sup>. The goal of these researches is to increase the accelerating gradients minimizing the probability of RF breakdown. Among the possible options, experimental results point out that metallic coatings of Transition Metal (TM) atoms may improve the properties of copper. The interplay of nano- and micrometer-scale factors is typically at the origin of the properties and the macroscopic behaviour of TM films, so that the capability to probe morphology and phase distribution of these complex systems at multiple length scale is mandatory. MoO<sub>3</sub> films are multiphase metallic systems with a not negligible contribution of disordered oxide phases: transparent and insulating phases such as MoO<sub>3</sub> or metallic phases such as MoO<sub>3</sub>, both of high-interest also for technological applications. Different chemical and structural factors may affect the properties of MoO<sub>3</sub> films and, in particular, the work function<sup>(17,18)</sup>. We have already studied thin films of MoO<sub>3</sub> growth by physical vapour deposition in vacuum<sup>(17,18)</sup>, here we will describe the molybdenum oxide (MoO<sub>3</sub>) films deposited by pulsed-laser deposition (PLD) and their preliminary mechanical characterization.

## 2 - PULSED-LASER DEPOSITION AND XRD CHARACTERIZATION OF MoO<sub>3</sub> FILMS

Molybdenum oxide (MoO<sub>3</sub>) thin films were deposited by pulsed-laser deposition (PLD) starting from a commercial MoO<sub>3</sub> target. In figure 1 we show the laser system available at the *Istituto Struttura della Materia* - CNR, a Nd:Yag operating at 355 nm with a pulse duration of 7 ns, an energy density of 2 J/cm<sup>2</sup> and a repetition rate of 10 Hz. The deposition chamber shown in figure 1 is a cylindrical volume with a top flange used as a viewport and with six lateral flanges. It is equipped with a multitarget system and with a substrate heater, which allows to deposit films up to temperatures of 900° C. During the deposition the target can be rotated to obtain more uniform films.



**FIG. 1** - The PLD apparatus: the vacuum chamber (left) and the Nd:Yag laser (right) (Colour on line).

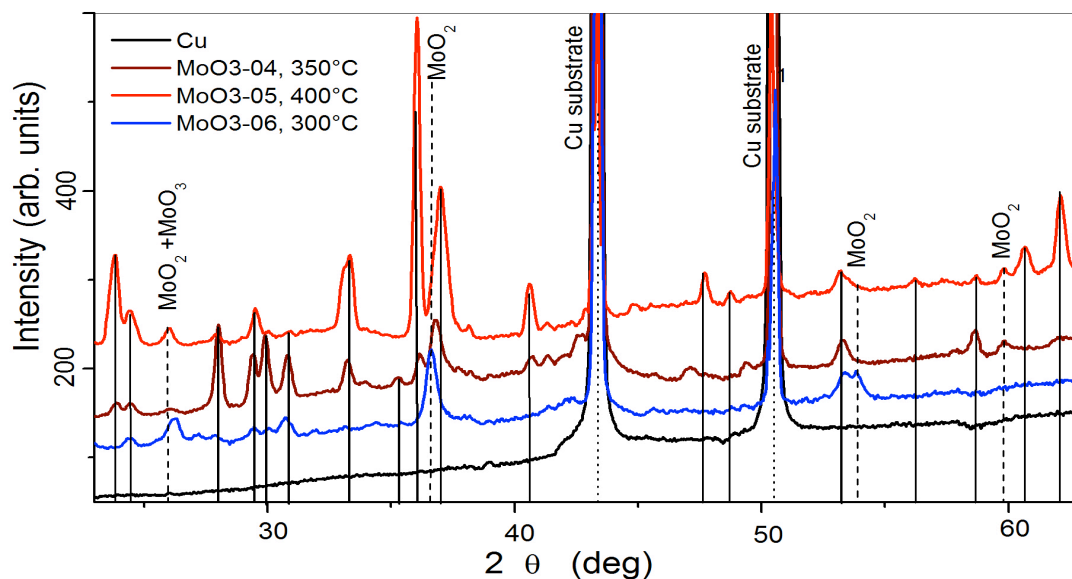
Six MoO<sub>3</sub> films were deposited onto smooth Cu substrates at different substrate temperature (T.),

ranging from 300° C to 400° C, as measured by the temperature controller and monitored by an optical pyrometer. The target to substrate distance was set to 5 cm. The deposition chamber was evacuated to a base pressure of  $10^{-7}$  mbar prior to film deposition and pure oxygen gas was introduced inside the chamber during the deposition. The oxygen partial pressure was in the range 0.01-0.2 mbar and also the deposition time was changed to study the effect of growth temperature on the structural and electrical characteristics of these films. In Table 1 are listed the deposition parameters of the films deposited by PLD.

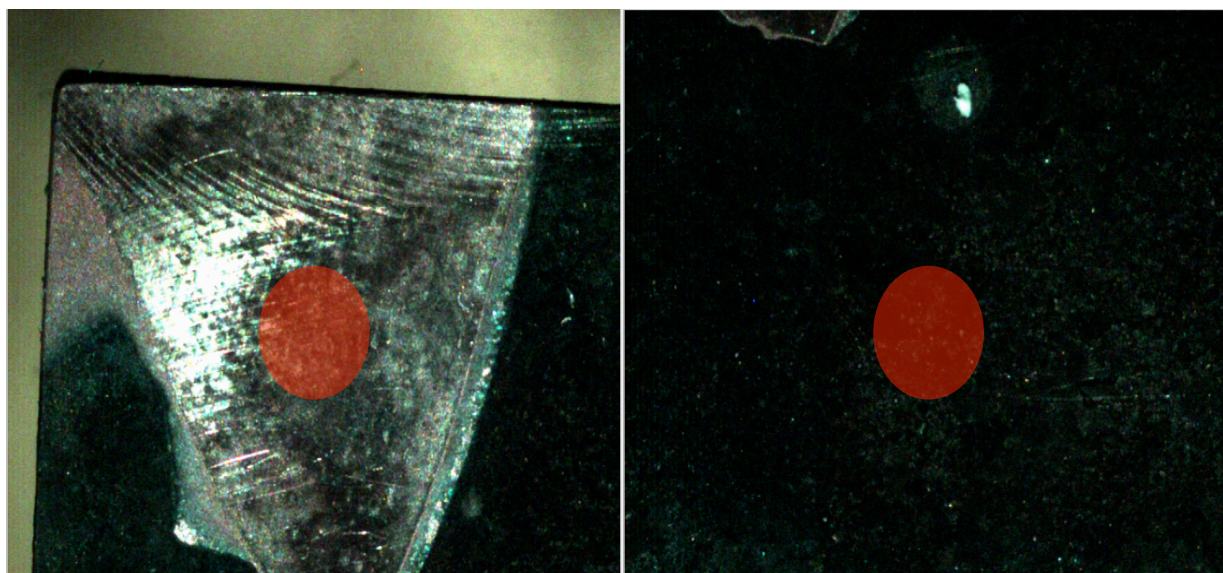
**TABLE 1** - List of the samples deposited by PLD.

| <b>Film</b>               | <b>T<sub>s</sub> (°C)</b> | <b>p(O<sub>2</sub>) (mbar)</b> | <b>Deposition time (min)</b> |
|---------------------------|---------------------------|--------------------------------|------------------------------|
| <i>MoO<sub>3</sub>-01</i> | 380                       | 10 <sup>-3</sup>               | 15                           |
| <i>MoO<sub>3</sub>-02</i> | 370                       | 2x10 <sup>-3</sup>             | 22                           |
| <i>MoO<sub>3</sub>-03</i> | 365                       | 10 <sup>-3</sup>               | 20                           |
| <i>MoO<sub>3</sub>-04</i> | 350                       | 10 <sup>-3</sup>               | 10                           |
| <i>MoO<sub>3</sub>-05</i> | 400                       | 2x10 <sup>-3</sup>             | 20                           |
| <i>MoO<sub>3</sub>-06</i> | 300                       | 2x10 <sup>-3</sup>             | 20                           |

In Figure 2 are compared XRD patterns of three films: MoO<sub>3</sub>-04, MoO<sub>3</sub>-05 and MoO<sub>3</sub>-06, collected with a Rigaku diffractometer in the Bragg-Brentano geometry using the Cu K<sub>α</sub> ( $\lambda = 1.5418$  Å) in the  $\theta$ -2 $\theta$  scan mode. The films grown at lower oxygen pressures (10<sup>-3</sup> mbar - not shown) mainly exhibit the peaks of the MoO<sub>3</sub> phase whereas at O<sub>2</sub> pressures of ~0.1 mbar also the peaks characteristic of the MoO<sub>3</sub> phase appear. The effect of the deposition temperature T<sub>s</sub>, at the O<sub>2</sub> pressure of 0.1 mbar, is evident from the XRD spectra: at 300° C and 20 minutes of deposition (MoO<sub>3</sub>-06) we observe a coexistence of both phases, whereas at 350° C and 10 minutes of deposition (MoO<sub>3</sub>-04) the MoO<sub>3</sub> phase prevails on the MoO<sub>3</sub> one. At T<sub>s</sub>= 400° C and 10 minutes of deposition (MoO<sub>3</sub>-05) the film mainly shows the presence of the MoO<sub>3</sub> phase with a high degree of crystallinity.



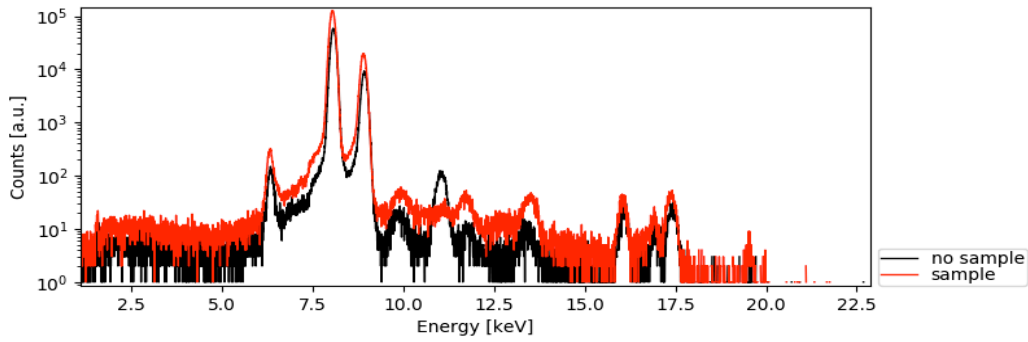
**FIG. 2** - XRD spectra of MoO<sub>3</sub> films deposited at different temperatures and deposition time ( $pO_2=0.1-0.2$  mbar). Continuous lines highlight the MoO<sub>3</sub> phase peaks, whereas dash and dot lines connect the MoO<sub>3</sub> (or mixed MoO<sub>3</sub> + MoO<sub>2</sub>) phase and the Cu substrate peaks, respectively (ref. JCPDF, 1997, cards 84-1360 and 78-1072) (Colour on line).



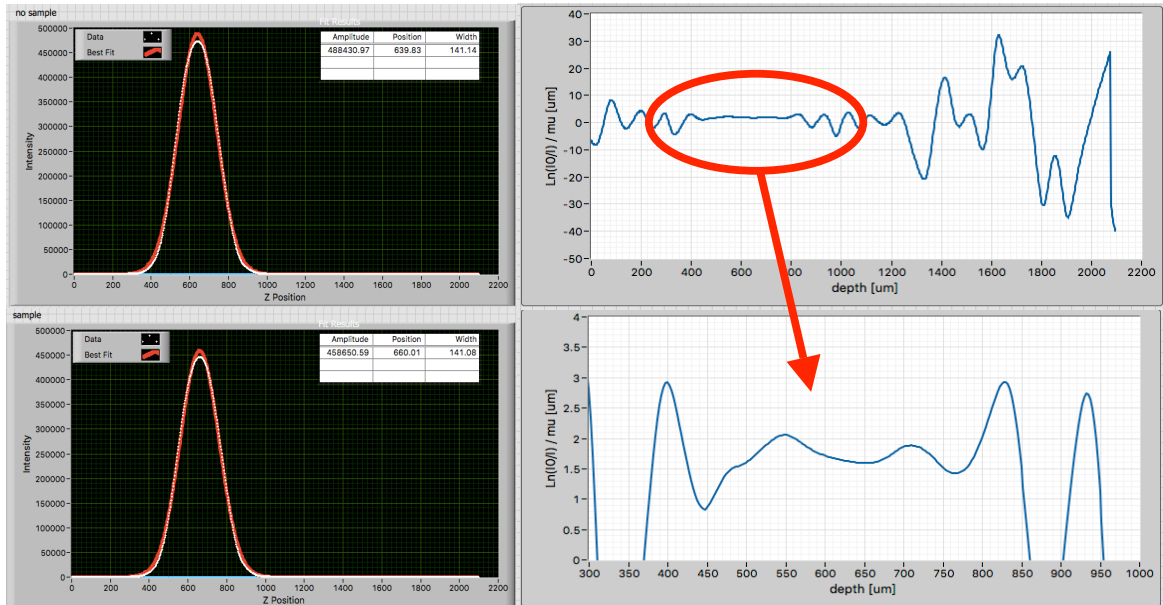
**FIG. 3** - The red spots in the two panels show the locations of the XRD measurement on the PLD coatings: copper (left) and MoO<sub>3</sub> (right) (Colour on line).

### 3 – MoO<sub>3</sub> FILMS ON COPPER

MoO<sub>3</sub> coated on copper by physical vapour deposition in vacuum without thermal annealing mainly growth as a disordered film<sup>(7,18)</sup>. To characterize the quality of films deposited by PLD we performed XRF experiments at the RXR facility of the Laboratori Nazionali di Frascati based on a confocal set that was characterized probing a spherical object of  $\sim 80 \mu\text{m}$  diameter<sup>(9)</sup>. The experimental parameters with the conventional molybdenum anode source are: time acquisition per point 180 sec,  $V = 40 \text{ kV}$  and  $I = 950 \mu\text{A}$ . To measure the coatings and the copper substrate we chosen two points, one on the copper surface and the other on the coated copper as showed in Figure 3. Actually, with this layout it is not possible to perform a quantitative analysis of the sample. However, thanks to the capacity of the RXR setup to perform a 3D analysis and thanks to the copper substrate, we performed the absorption fluorescence analysis by a depth scan.



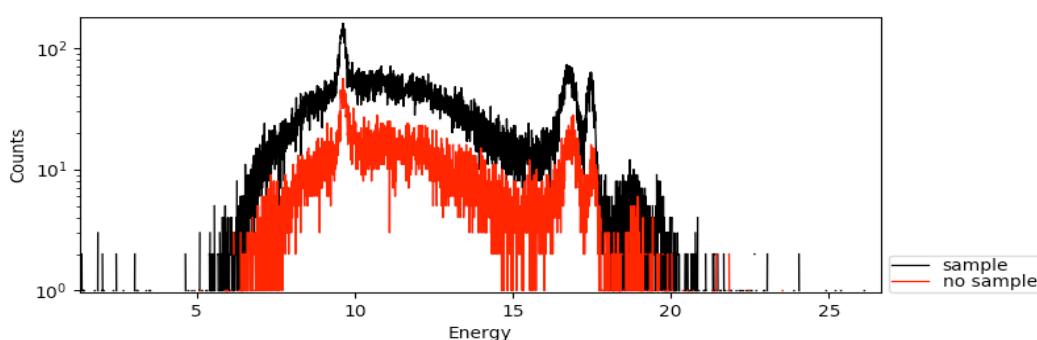
**FIG. 4** - Comparison of XRF spectra of the MoO<sub>3</sub> (red) and of the copper (black) (Colour on line).



**FIG. 5** - (left) Integrated Cu fluorescence data vs. depth: Cu (top) and Cu/MoO<sub>3</sub> (below) as showed in Figs. 3,4; (right) plots show the path length obtained by Moseley equation (Colour on line).

In Figure 4 are compared the two spectra collected on copper and on the oxide coating. Peaks with similar relative intensities appear at 9.8, 11, 11.5, 13 and 16 keV, at variance of the peak at 11 keV, which is stronger on the copper surface. According to this, taking into account the Cu peak we performed an absorption study to evaluate the thickness of the  $\text{MoO}_3$ . In particular, we have evaluated the peak area for each position vs. depth, i.e., along the Z axis, measuring the beam intensity with and without the coated film. From the Cu fluorescence intensity ratio, i.e., from the  $I_0/I$  ratio of the Moseley law<sup>30)</sup> assuming to know the absorption coefficient of  $\text{MoO}_3$ , we can estimate the sample thickness. In the left panel of Figure 5 is shown the integrated Cu fluorescence intensities vs. depth, while in the right panel we showed the path length obtained by the Moseley equation.

To evaluate the film thickness, we have to consider in Figure 5 only the region highlighted in red where the confocal probe starts to enter in the sample, i.e.,  $> 400 \mu\text{m}$ . Data are stable and constant for  $\sim 400 \mu\text{m}$ , after while the probe is totally absorbed by the copper substrate. In the flat region in the top right panel correspond to  $1.71 \pm 0.45 \mu\text{m}$  and can be interpreted as the path that the fluorescence radiation travels from the copper substrate to reach the surface of the film. Since the radiation is not hitting the surface along the normal<sup>19)</sup>, from trigonometrical consideration we can obtain both  $l$ , the path travelled by the fluorescence radiation inside the film and then the thickness  $x = 0.86 \pm 0.30 \mu\text{m}$  of the  $\text{MoO}_3$  film. Using the same technique, we evaluated the  $\text{MoO}_3$  thickness of one film coated on sapphire. In figure 6 are compared the XRF spectrum of the  $\text{MoO}_3$  film growth on the substrate of sapphire with the XRF spectrum without film. Actually, since the copper substrate is replaced by the sapphire and due to the very low efficiency of the RXR confocal setup at low energy, we cannot apply the same method to evaluate the thickness of the coating. In addition, fluorescence measurements, showed the presence of zinc, about one order of magnitude more intense in the coating than in the substrate, not observed in the previous case.



**FIG. 6** - Comparison of XRF spectra of  $\text{MoO}_3$  (red) and sapphire (black) (Colour on line).


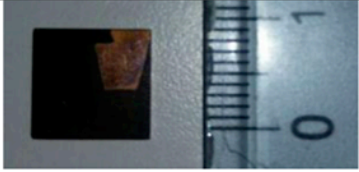
#### 4 – STUDY OF MECHANICAL PROPERTIES OF $\text{MoO}_3$ FILMS ON COPPER

The study of mechanical properties of  $\text{MoO}_3$  films showed in Figure 7 has been performed at the LIME laboratory of the Roma Tre University using the Confocal Optical Profiling and Nanoindentation analysis. The analysis has been performed with the parameters in Table 2:



**TABLE 2** - The input parameters of the confocal optical profiling analysis.

|             |              |
|-------------|--------------|
| Tip         | Berkovich    |
| Mode        | Standard CSM |
| Indentation | 5x3 matrix   |
| Max. depth  | 500 nm       |

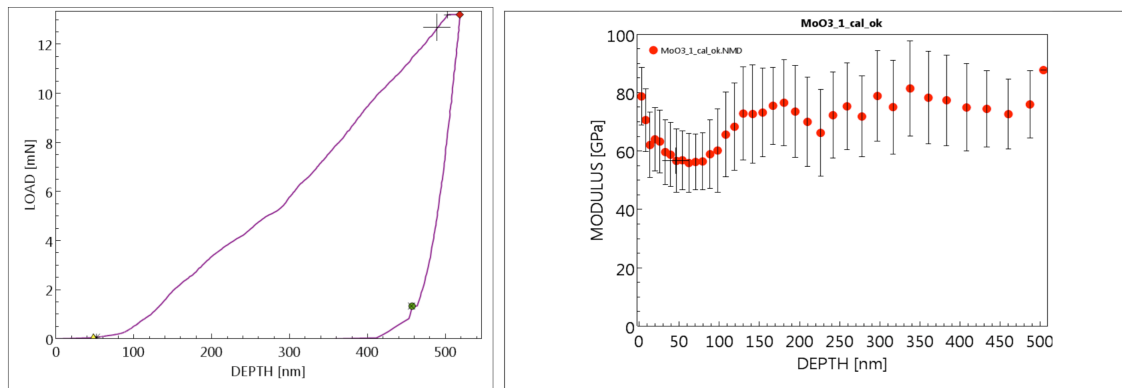
| Campione | Immagine   | Codice originale     |
|----------|--|----------------------|
| #1       |  | MoO <sub>3</sub> -01 |
| #2       |   | MoO <sub>3</sub> -02 |

**FIG. 7** - Photographs of the MoO<sub>3</sub>-01 and MoO<sub>3</sub>-02 films on copper (Colour on line).

As reported in the Table 3 the analysis of the MoO<sub>3</sub>-01 and MoO<sub>3</sub>-02 films (see additional information in Appendix 1) returns a higher roughness for the MoO<sub>3</sub>-01 sample with respect to MoO<sub>3</sub>-02 sample.

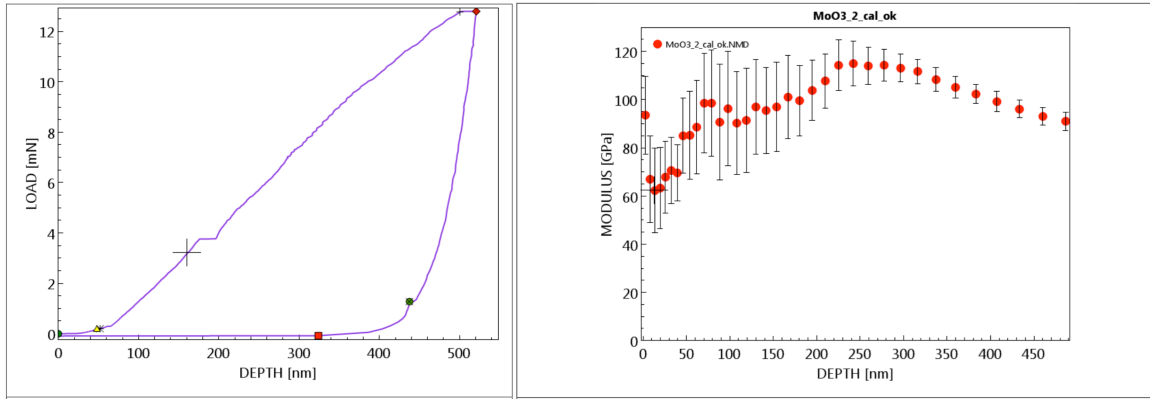
**TABLE 3** - The roughness parameters of the MoO<sub>3</sub>-01 and MoO<sub>3</sub>-02 films

| Sample               | Sa (μm) | Ra (μm)     |
|----------------------|---------|-------------|
| MoO <sub>3</sub> -01 | 0.201   | 0.175±0.035 |
| MoO <sub>3</sub> -02 | 0.115   | 0.083±0.019 |



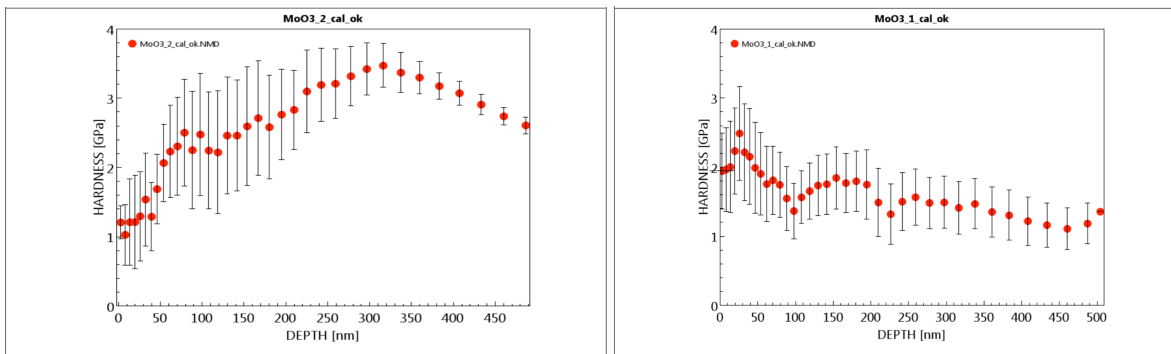
**FIG. 8** - MoO<sub>3</sub>-01 - (left) the load and (right) the modulus as function of depth (Colour on line).

Concerning the hardness and the elastic modulus we measured them as function of the depth for both samples. The following figures show the plots of the load and of the modulus and of these two samples.



**FIG. 9** - MoO3-02 - (left) the load and (right) the modulus as function of depth (Colour on line).

The hardness and elastic modulus values of these films can be extrapolated from the *zero* value of depth (x axis) in the plot or as the average of the three first measured values (figures 8-10). The results of the mechanical analysis depend by the copper substrate conditions. In spite the two samples analyzed have the same copper substrate, they show different hardness value related to the maximum depth. This result is likely due to the different parameters of the PLD process. The elastic modulus and the hardness as function of depth highlight the dependence on roughness, thickness and homogeneity of these molybdenum oxide films and of the substrate.



**FIG. 10** - The hardness vs. depth for MoO3-01 (left) and MoO3-02 films (right) (Colour on line).

## 5 – CONCLUSIONS

In this document we report an investigation of temperature and  $O_2$  pressure conditions for the growth of  $MoO_3$  films by PLD starting from  $MoO_3$  targets. The interest for these films is due to the peculiar electrical and electronic characteristics of  $MoO_3$ : in fact, due to the high work function (7 eV) and insurgence of conductive layers when grown on thick copper substrates [17], these films could be very promising to solve many of the issues in accelerating cavities at high field gradients.

We found that for these nanophase oxide films with a thickness higher than 1  $\mu m$  as derived from XRF spectra, the presence of a  $MoO_3$  phase with a high crystallinity degree is obtained when the substrate is heated at the temperature of 400° C and with the  $O_2$  pressure of 0.1 mbar. For these films the mechanical characterizations of hardness and elastic modulus show a dependence on the maximum depth. Efforts are needed to improve the homogeneity of the film thickness and, in particular, to improve the roughness, which is associated to the different behaviours of the different oxide phases. Finally, in order to prevent possible contaminations or oxidations, we underline that the vacuum in the deposition chamber has to be  $\sim 10^{-8}$  mbar or less. Characterizations of  $MoO_3$  films with thickness  $> 1 \mu m$  on copper substrates are planned to check stability, mechanical resistance and chemical properties of these molybdenum oxide films.

## 6 – ACKNOWLEDGEMENTS

We kindly acknowledge C. Veroli for his support in the XRD measurements. A special thanks is due to E. Benporad of the Roma TRE Electron Microscopy Laboratory (LIME).

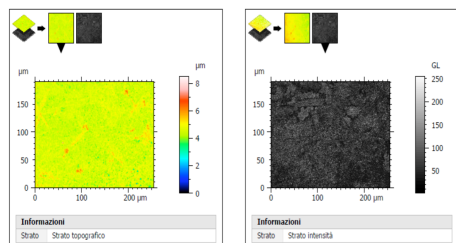
## REFERENCES

- (1) T.E. Graedel, E.M. Harper, N.T. Nassar, and B.K. Reck, On the materials basis of modern society. *Proceedings of the National Academy of Sciences*, 112(20), 6295–6300; 2013
- (2) D.P. Pritzkau and R.H. Siemann, Experimental study of rf pulsed heating on oxygen free electronic copper. *Phys. Rev. Special Topics - Accelerators and Beams*, 5(11); 2002
- (3) S. Döbert, C. Adolphsen, G. Bowden, D. Burke, J. Chan, V. Dolgashev, J. Frisch, K. Jobe, R. Jones, J. Lewandowski, R. Kirby, Z. Li, D. McCormick, R. Miller, C. Nantista, J. Nelson, C. Pearson, M. Ross, D. Schultz, T. Smith, S. Tantawi, J. Wang, T. Arkan, C. Boffo, H. Carter, I. Gonin, T. Khabiboulline, S. Mishra, G. Romanov, N. Solyak, Y. Funahashi, H. Hayano, N. Higashi, Y. Higashi, T. Higo, H. Kawamata, T. Kume, Y. Morozumi, K. Takata, T. Takatomi, N. Toge, K. Ueno, Y. Watanabe, High Gradient Performance of NLC/GLC X-Band Accelerating Structures, *Proceedings of the 2005 Particle Accelerator Conference*; 2005
- (4) S. Bini, V. Chimenti, A. Marcelli, L. Palumbo, B. Spataro, V.A. Dolgashev, S. Tantawi, A.D. Yeremian, Y. Higashi, M.G. Grimaldi, L. Romano, F. Ruffino, R. Parodi, Development of X-band accelerating structures for high gradients, *CPC (HEP & NP)*, 36(7): 639–647; 2012
- (5) T. Kwan, J.M. Dawson and A.T. Lin, Free electron laser. *Phys. Fluids* 20(4), 581; 1977
- (6) D.A.G. Deacon, L.R. Elias, J.M.J. Madey, G.J. Ramian, H.A. Schwettman and T.I. Smith, First Operation of a Free-Electron Laser. *Phys. Rev. Lett.* 38(16), 892–894; 1977
- (7) C.Z. Antoine, F. Peauger, F. Le Pimpec, Electromigration occurrences and its effects on metallic surfaces submitted to high electromagnetic field: A novel approach to breakdown in accelerators. *Nucl. Instrum. Methods Phys. Res. Sect. A* 665 (2011) 54–69.

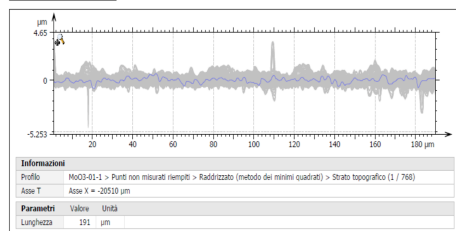


- (8) J. Knobloch, *Advanced Thermometry Studies of Superconducting Radio Frequency Cavities*, 1997, Cornell University. p. 285.
- (9) Norem, J., Z. Insepov, and I. Konkashbaev, Triggers for RF breakdown. *Nuclear Instruments and Methods in Physics Research Section A: Accelerators, Spectrometers, Detectors and Associated Equipment*, 2005. 537(3): p. 510-520.
- (10) Z. Insepov, et al., Modeling RF breakdown arcs. *Cornell University Library* 2011 (4).
- (11) V.A. Dolgashev, et al., RF breakdown in normal conducting single-cell structures. in *Particle Accelerator Conference 2005*. Knoxville.
- (12) J.W. Wang and SLAC. *R&D of Accelerator Structures at SLAC*. United States: N.p., 2007
- (13) Ed. G. Guignard, CLIC Study Team, CERN 2000-008, 2000
- (14) E. Belli, P. Costa Pinto, G. Rumolo, A. Sapountzis, T. Sinkovits, M. Taborelli, B. Spataro, M. Zobov, G. Castorina and M. Migliorati, Electron cloud buildup and impedance effects on beam dynamics in the Future Circular e-e Collider and experimental characterization of thin TiZrV vacuum chamber coatings, *Phys. Rev. Acc. Beams* 21, 111002 (2018)
- (15) A. Marcelli, B. Spataro, S. Sarti, V.A. Dolgashev, S. Tantawi, D.A. Yeremian, Y. Higashi, R. Parodi, A. Notargiacomo, J. Xu, G. Cappuccio, G. Gatti, G. Cibir, *Surf. Coat. Tech.* 261 (2015) 391-397
- (16) A. Marcelli, B. Spataro, G. Castorina, W. Xu, S. Sarti, F. Monforte, G. Cibir, *Condensed Matter* 2 (2017) 18; doi:10.3390/condmat2020018
- (17) S. Macis, C. Aramo, C. Bonavolontà, G. Cibir, A. D'Elia, I. Davoli, M. De Lucia, M. Lucci, S. Lupi, M. Miliucci, A. Notargiacomo, C. Ottaviani, C. Quaresima, M. Scarselli, J. Scifo, B. Spataro, M. Valentino, P. De Padova and A. Marcelli. *MoO<sub>3</sub> films grown on polycrystalline Cu: morphological, structural and electronic properties*” *J. Vacuum Sci. Tech. A* (2018) in press
- 18. S. Macis, Deposition and characterization of thin MoO<sub>3</sub> films on Cu for technological applications, XXXI cycle (2018) Tor Vergata University, Rome.
- 19. D. Hampai, Yu.M. Cherepennikov, A. Liedl, G. Cappuccio, E. Capitolo, M. Iannarelli, C. Azzutti, Yu.P. Gladkikh, A. Marcelli and S.B. Dabagov, Polycapillary based  $\mu$ XRF station for 3D colour tomography, *JINST* 13, C04024 (2018).
- 20. H.G.J. Moseley, H.G. Jeffreys. "XCIII. The high-frequency spectra of the elements." *The London, Edinburgh, and Dublin Philosophical Magazine and Journal of Science* 26.156 (1913): 1024-10

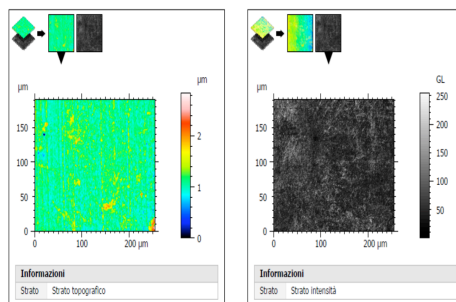
## APPENDIX 1



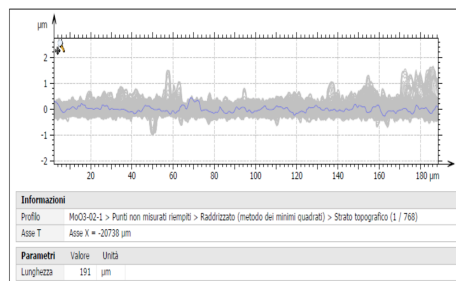
| ISO 25178            |          |
|----------------------|----------|
| Parametri di altezza |          |
| Sq                   | 0.274 µm |
| Ssk                  | 0.799    |
| Sku                  | 10.6     |
| Sp                   | 3.98 µm  |
| Sv                   | 4.52 µm  |
| Sz                   | 8.51 µm  |
| Sa                   | 0.201 µm |



|   |    | Contesto   | Medio | Dev std | Min   | Max   |
|---|----|--|-------|---------|-------|-------|
| ISO 4287  |    |  |       |         |       |       |
| Parametri di ampiezza - Profilo di rugosità           |    |  |       |         |       |       |
| Rp  | µm | Filtro di Gauss, 0.08 mm                                   | 0.658 | 0.342   | 0.224 | 3.59  |
| Rv  | µm | Filtro di Gauss, 0.08 mm                                   | 0.586 | 0.187   | 0.273 | 2.04  |
| Rz  | µm | Filtro di Gauss, 0.08 mm                                   | 1.24  | 0.397   | 0.641 | 4.09  |
| Rc  | µm | Filtro di Gauss, 0.08 mm, ISO 4287 senza emendamento 2     | 0.549 | 0.112   | 0.338 | 1.21  |
| Rt  | µm | Filtro di Gauss, 0.08 mm                                   | 1.35  | 0.392   | 0.735 | 4.09  |
| Ra  | µm | Filtro di Gauss, 0.08 mm                                   | 0.175 | 0.0355  | 0.113 | 0.290 |
| Rq  | µm | Filtro di Gauss, 0.08 mm                                   | 0.228 | 0.0534  | 0.140 | 0.521 |
| Rsk   |    | Filtro di Gauss, 0.08 mm                                   | 0.229 | 0.856   | -2.49 | 5.54  |
| Rku   |    | Filtro di Gauss, 0.08 mm                                   | 4.08  | 3.42    | 1.97  | 40.6  |
| Parametri di rapporto materiale - Profilo di rugosità |    |  |       |         |       |       |
| Rmr   | %  | c = 1 µm sotto il picco più alto, Filtro di Gauss, 0.08 mm | 82.3  | 25.9    | 0.595 | 100   |
| Rdc   | µm | p = 20%, q = 80%, Filtro di Gauss, 0.08 mm                 | 0.351 | 0.0576  | 0.231 | 0.575 |



| ISO 25178            |          |
|----------------------|----------|
| Parametri di altezza |          |
| Sq                   | 0.159 µm |
| Ssk                  | 1.41     |
| Sku                  | 11.5     |
| Sp                   | 1.75 µm  |
| Sv                   | 1.39 µm  |
| Sz                   | 2.84 µm  |
| Sa                   | 0.115 µm |



|   |    | Contesto   | Medio  | Dev std | Min    | Max   |
|---|----|--|--------|---------|--------|-------|
| ISO 4287  |    |  |        |         |        |       |
| Parametri di ampiezza - Profilo di rugosità           |    |  |        |         |        |       |
| Rp  | µm | Filtro di Gauss, 0.08 mm                                   | 0.321  | 0.146   | 0.134  | 1.30  |
| Rv  | µm | Filtro di Gauss, 0.08 mm                                   | 0.270  | 0.112   | 0.107  | 1.02  |
| Rz  | µm | Filtro di Gauss, 0.08 mm                                   | 0.591  | 0.212   | 0.307  | 1.76  |
| Rc  | µm | Filtro di Gauss, 0.08 mm, ISO 4287 senza emendamento 2     | 0.274  | 0.0709  | 0.140  | 0.614 |
| Rt  | µm | Filtro di Gauss, 0.08 mm                                   | 0.665  | 0.222   | 0.315  | 1.76  |
| Ra  | µm | Filtro di Gauss, 0.08 mm                                   | 0.0833 | 0.019   | 0.0487 | 0.171 |
| Rq  | µm | Filtro di Gauss, 0.08 mm                                   | 0.109  | 0.0305  | 0.0653 | 0.275 |
| Rsk   |    | Filtro di Gauss, 0.08 mm                                   | 0.353  | 0.658   | -1.67  | 3.09  |
| Rku   |    | Filtro di Gauss, 0.08 mm                                   | 3.81   | 1.71    | 2.08   | 14.3  |
| Parametri di rapporto materiale - Profilo di rugosità |    |  |        |         |        |       |
| Rmr   | %  | c = 1 µm sotto il picco più alto, Filtro di Gauss, 0.08 mm | 98.7   | 8.95    | 9.52   | 100   |
| Rdc   | µm | p = 20%, q = 80%, Filtro di Gauss, 0.08 mm                 | 0.169  | 0.0304  | 0.104  | 0.262 |

FIG. A1 - The roughness analysis of MoO3-01 (top) and of MoO3-02 films (below) (Colour on line).